This is the accepted manuscript made available via CHORUS. The article has been published as:

Length scale of interaction in spatiotemporal chaos

Dan Stahlke and Renate Wackerbauer

Phys. Rev. E **83**, 046204 — Published 8 April 2011

DOI: 10.1103/PhysRevE.83.046204

Length Scale of Interaction in Spatiotemporal Chaos

Dan Stahlke* and Renate Wackerbauer†
Department of Physics, University of Alaska, Fairbanks, Alaska 99775-5920, USA

Extensive systems have no long scale correlations and behave as a sum of their parts. Various techniques are introduced to determine a characteristic length scale of interaction beyond which spatiotemporal chaos is extensive in reaction-diffusion networks. Information about network size, boundary condition or abnormalities in network topology gets scrambled in spatiotemporal chaos, and the attenuation of information provides such characteristic length scales. Space-time information flow associated with the recovery of spatiotemporal chaos from finite perturbations, a concept somewhat opposite to the paradigm of Lyapunov exponents, defines another characteristic length scale. High-precision computational studies of asymptotic spatiotemporal chaos in the complex Ginzburg-Landau system and transient spatiotemporal chaos in the Gray-Scott network show that these different length scales are comparable and thus suitable to define a length scale of interaction. Preliminary studies demonstrate the relevance of these length scales for stable chaos.

PACS numbers: 05.45.Jn, 05.45Xt

I. INTRODUCTION

Spatiotemporal chaos (STC) is a generic pattern in extended non-equilibrium systems exhibiting a rapid decay of spatial and temporal correlations [1]. Asymptotic STC is reported for example in fluid experiments [2], chemical reaction-diffusion systems [3], and in cardiac fibrillation [4]. In transient STC the spatiotemporal dynamics spontaneously collapses into a regular behavior [5]; manifestations include turbulence in shear flow [6], models for semiconductor charge transport [7], or chemical reaction-diffusion models [8, 9].

STC is characterized by sensitivity to initial conditions; infinitesimal perturbations grow on average exponentially in time to yield a positive Lyapunov exponent. Lorenz famously described the possibility that the flap of a butterfly's wings in Brazil may set off a tornado in Texas [10]. Although perturbations certainly have a course-altering impact on the evolution of the entire system, they will leave no observable mark on the system's long term space-time behavior; information about these perturbations quickly becomes lost. I.e., although the flap of a butterfly's wings in Brazil may set off a tornado in Texas, the citizens of Texas have no way of knowing of the existence of the butterfly from solely observing the weather. It would be absurd for the citizens of Brazil and Texas to attempt to communicate through butterflies and tornados.

Even though every part of an STC system has the ability to change the evolution of the entire system, there exists an effective decoupling between distant parts; this can be quantified with correlation length scales [1, 11], time-delayed mutual information between distant points [12, 13], or transfer entropy [14]. This decoupling directly relates to Ruelle's claim [15] that extended chaotic systems without long-range interactions are uncorrelated at large length scales and therefore should behave as a sum of their parts. Then STC is extensive, and the attractor dimension grows in direct proportion to the volume of the system [1, 16]. If this linear relation is fulfilled for small changes of system size, STC is said to be microextensive [17]. Lyapunov dimension, sum of positive Lyapunov exponents, and the logarithm of the average lifetime in the case of transient STC have been reported to be extensive in large systems [7–9, 11, 17–24]. STC in small extended systems can exhibit significant deviations from microextensivity in Lyapunov dimension [25].

This paper introduces and explores various techniques to determine a characteristic length scale beyond which STC is extensive in reaction-diffusion networks. For systems much larger than this characteristic length scale the local dynamics is independent of the system size and microextensivity is expected. We also find that irregularities in the network topology (boundary condition, network shortcut) do not influence the system characteristics much beyond this length scale. Several candidates for this length scale will be presented, and *length scale of interaction* should be understood to mean an order-of-magnitude value that could refer to any one of these. Section II introduces the two models, the complex Ginzburg-Landau (cGL) reaction-diffusion network with asymptotic STC and the Gray-Scott reaction-diffusion network with transient STC. Section III provides candidates for the length scale of interaction based on time-averaged system variables. The information flow in reaction-diffusion networks is discussed in Sect. IV via transfer entropy. In Sect. V space-time information flow is probed with finite bump perturbations and measured with particular space-time averages. Section VI discusses the relevance of these length scales of interaction for stable chaos in a coupled map lattice. A discussion of the results is presented in Sect. VII.

II. REACTION DIFFUSION NETWORKS EXHIBITING SPATIOTEMPORAL CHAOS

The network consists of N diffusively coupled, identical, continuous-time dynamical elements,

$$\frac{d\mathbf{x}_n}{dt} = \mathbf{F}(\mathbf{x}_n) + DH \sum_{j=1}^{N} \Delta_{nj}\mathbf{x}_j. \tag{1}$$

* dstahlke@gmail.com
† rawackerbauer@alaska.edu

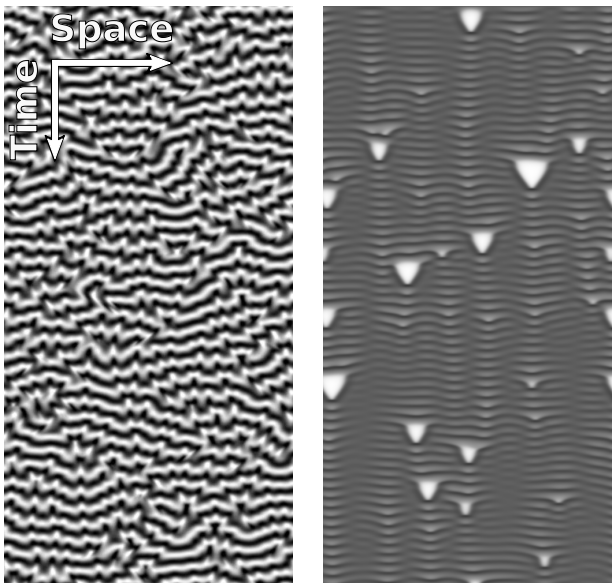

(a) (b)

FIG. 1. Spatiotemporal chaos of the variable a in the (a) complex Ginzburg-Landau (cGL) ring network and in the (b) transient phase of the Gray-Scott (GS) ring network. The cGL system is plotted for 300 time units, $N = 500$ nodes, and for the parameters $c_1 = 3.5$, $c_3 = 0.95$, and $D = 4$. The GS system is plotted for 300 time units, $N = 500$ nodes, and for the parameters $\mu = 33.7$, $\Phi = 2.8$, and $D = 16$. A 4^{th} order Runge-Kutta integration method was used; large values of a are color coded in white.

At each network node $n\,(n = 1, 2, \ldots N)$ the local dynamics is given by $\mathbf{F}(\mathbf{x}_n)$ with $\mathbf{x}_n$ a d-dimensional state vector and $\mathbf{F} : R^d \to R^d$ a function. The diffusive coupling term depends on the global coupling parameter D, and on the $d \times d$ matrix H, which controls the relative diffusion and mixing of the d components of $\mathbf{x}_n$. Δ is a discrete $N \times N$ symmetric Laplacian matrix required to meet the condition $\sum_{j=1}^{N} \Delta_{ij} = 0$. The network topology and boundary conditions are defined by Δ [20].

Equation (1) is approximately invariant under the variation of N and D with $N/\sqrt{D}$ fixed. If N goes to infinity with $N/\sqrt{D}$ held constant, the system approaches a continuous form. On the other hand if N (and hence D) is made too small, discretization effects will become significant and eventually the system will no longer support chaos. D controls the characteristic length scale; it is chosen large enough for the networks to be good approximations for the continuum system [20].

We consider two dynamical systems, the complex Ginzburg-Landau (cGL) system [1, 26] and the Gray-Scott (GS) system [27]. The dynamical state of each of these systems consists of two real variables per node ($d = 2$); thus, spatiotemporal chaos is induced by the diffusive coupling of the non-chaotic dynamical elements.

The *complex Ginzburg-Landau system* describes a wide range of physical phenomena including aspects of superconductivity, superfluidity, Bose-Einstein condensation, and liquid crystals [26]. It represents a normal form for a transition between a stationary homogeneous state to an oscillatory state close to a Hopf bifurcation [1]. In the cGL system the two-dimensional real system state $\mathbf{x}_n$ [Eq. (1)] is usually described by a single complex variable z_n; the equations are

$$\frac{d}{dt}z_n = z_n - (1 - ic_3)|z_n|^2 z_n + D(1 + ic_1)\sum_{j=1}^{N} \Delta_{nj} z_n. \quad (2)$$

The multiplicative factor $1+ic_1$ corresponds to the 2×2 matrix H in Eq. (1) for the real states. For consistency with the GS system we define the two real variables, $a_n := \Re(z_n)$ and $b_n := \Im(z_n)$.

For parameters above the Benjamin-Feir instability line, $c_1 c_3 = 1$, plane wave solutions are linearly unstable; phase turbulence as well as defect chaos [Fig. 1(a)] exists. Very recently, transient spatiotemporal chaos was reported for parameters below that instability line [18]. We have used the parameters $D = 4$, $c_1 = 3.5$ and $c_3 \in \{0.85, 0.95, 1.2\}$ to match the cases studied by Fishman and Egolf [25]. In this range of parameters the system exhibits defect chaos: spacetime dislocations where a constant phase line stops appear irregularly. The equal-time two-point correlation length of a decreases by a factor of about 20 across the range of parameters from $c_3 = 0.85$ to $c_3 = 1.2$ [25]. The uncoupled systems exhibit an unstable focus at the origin ($a_n = b_n = 0$), surrounded by a stable limit cycle of radius 1.

The *Gray-Scott system* [27] represents an open autocatalytic reaction $A + 2B \to 3B$ and $B \to C$. The equations are

$$\begin{aligned} \frac{d}{dt}a_n &= 1 - a_n - \mu a_n b_n^2 + D\textstyle\sum_{j=1}^{N} \Delta_{nj} a_n \\ \frac{d}{dt}b_n &= \mu a_n b_n^2 - \phi b_n + D\textstyle\sum_{j=1}^{N} \Delta_{nj} b_n. \end{aligned} \quad (3)$$

where a_n and b_n are the dimensionless species concentrations of A and B at node n, and ϕ and μ are bifurcation parameters. We use the well studied parameters $D = 16$, $\mu = 33.7$ and $\Phi = 2.8$.

In the GS system spatiotemporal chaos is transient [9] with the transient lifetime increasing exponentially with the network size N. Figure 1(b) shows a typical spatiotemporal pattern during the transient phase. Within the parameter regime of transient spatiotemporal chaos, the uncoupled system is characterized by a stable node, a saddle and an unstable focus. Spatiotemporal chaos in the coupled system is Šilnikov-like; a typical trajectory at a network node spirals away from the unstable focus toward the stable node, to be reinjected into the neighborhood of the unstable focus by the propagating reaction-diffusion front [28].

A *spatiotemporally chaotic system is extensive* if it has no long-range correlations and behaves as a sum of its parts. The Lyapunov dimension $D_{\mathcal{L}}$ grows then linearly with the size N of the network [1, 15, 16]. If this linearity is exactly fulfilled, even for arbitrarily small changes in size, then spatiotemporal chaos is called *microextensive* [17]. As system parts only interact weakly, a natural chaotic length scale ξ_δ was defined by Cross and Hohenberg [1] that describes the size (number of nodes) of a single degree of freedom,

$$\xi_\delta = \lim_{N\to\infty} \frac{N}{D_{\mathcal{L}}}. \quad (4)$$

Earlier studies reported that spatiotemporal chaos in the cGL system is extensive in Lyapunov dimension for large system sizes [11]. For small system sizes significant deviations from microextensivity exist in form of oscillations of the Lyapunov dimension with system size [25]. These oscillations were attributed to the existence of building blocks with the length scale of the oscillations determining the number of nodes of a building block. The magnitude of the deviations from microextensivity decrease exponentially with system size. Transient spatiotemporal chaos in the GS network is extensive; the Lyapunov dimension, the sum of positive Lyapunov exponents, as well as the logarithm of the average transient lifetime increase linearly with the network size [20]. Whether transient STC is microextensive for small network sizes is currently not known because of the short transient lifetimes for small networks. We find that ξ_δ varies between 6 and 10 nodes for the cGL network, and $\xi_\delta = 16$ nodes for the GS network (Table I) [29].

III. MEASURING LENGTH SCALE OF INTERACTION WITH NODE AVERAGES

Perhaps the simplest measure of the characteristics of a local region of a spatiotemporal system is the time averaged value of a variable X at node n [30], given by

$$\langle X_n \rangle = \lim_{T\to\infty} T^{-1} \int_0^T X_n dt. \tag{5}$$

The convergence of the computational estimate for $\langle X_n \rangle$ is slow and very large T are required to achieve the desired precision [31]. A parallel code is applied that computes the average over several different initial conditions and smaller T.

The local averages define a global spatiotemporal average,

$$\bar{X} = N^{-1} \sum_{n=1}^{N} \langle X_n \rangle . \tag{6}$$

For a chaotic system governed by equations with translational spatial symmetry (e.g., the GS ring network during the transient phase, or the cGL ring network) it should typically [32] be the case that $\bar{X} = \langle X_n \rangle$. For a large enough ring network $\bar{X}$ can be interpreted as representing the characteristics of the natural system behavior without the influence of boundary conditions or other non-homogeneous elements. For an infinitely large ring network a global average $\bar{X}_0$ is defined as

$$\bar{X}_0 = \lim_{N\to\infty} \bar{X}. \tag{7}$$

This value is used as a baseline against which deviations from ordinary behavior can be defined. For the purposes of this paper a good estimate for $\bar{X}_0$ was achieved with $N = 1000$.

In a *ring network (having translational node symmetry)* the average characteristics of dynamical variables $\bar{X}$ depends on the size of the network, but converges quickly to the limiting value $\bar{X}_0$. Figure 2 reveals that the deviations of spacetime averages between small and large ring networks, $|\bar{X} - \bar{X}_0|$, decrease exponentially with the network size N for both systems

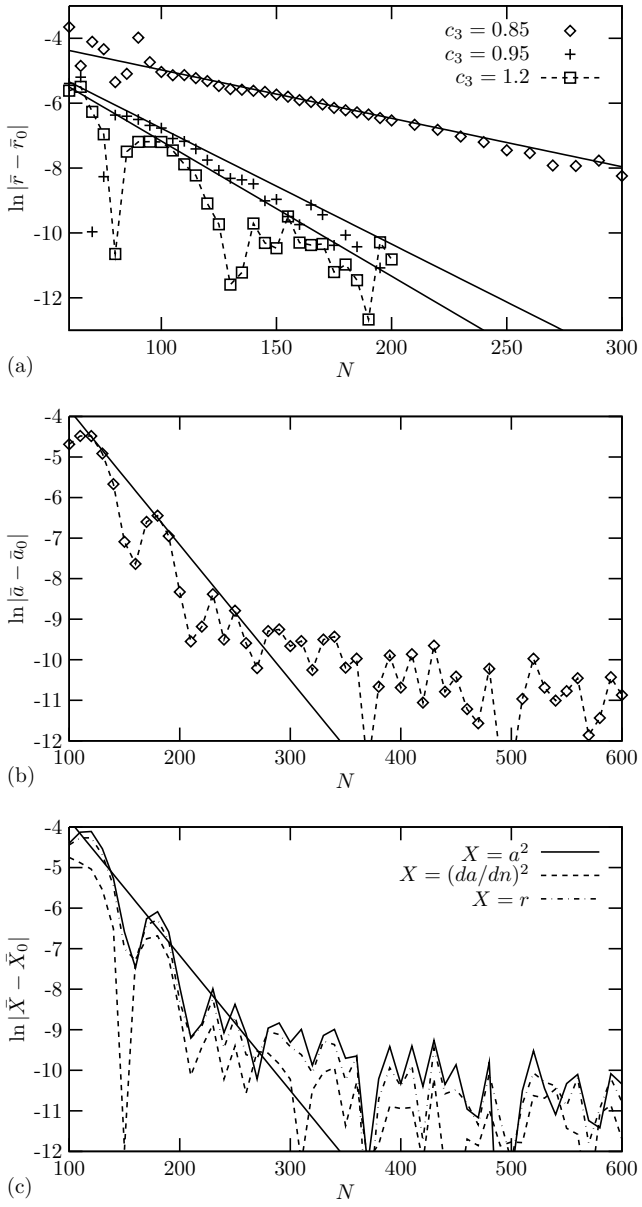

FIG. 2. Deviation of spacetime averages [$\bar{X}$, Eq. (6)] from those of a large ($N = 1000$) ring network [$\bar{X}_0$, Eq. (7)] as a function of network size N: (a) $\ln|\bar{r} - \bar{r}_0|$ for the cGL ring network ($c_1 = 3.5, c_3 \in \{0.85, 0.95, 1.2\}$) with $r = |z|$ the distance to the unstable focus; (b) $\ln|\bar{a} - \bar{a}_0|$ for the GS ring network ($\mu = 33.7, \Phi = 2.8$); (c) $\ln|\bar{X} - \bar{X}_0|$ for the same GS ring network as in (b) and different variables X ($X = a^2$, $X = (da/dn)^2$, and $X = r$ with r the distance to the unstable focus). The envelopes of the curves in (a) and (b) are fitted with a subjectively chosen linear function. The linear fit from (b) is copied into (c) to guide the eye. The deviations of spacetime averages in Fig. (a) do not match the deviations from extensivity of the Lyapunov dimension in [25].

(cGL, GS) and for a wide variety of variables X. In all cases the corresponding linear trend in $\ln|\bar{X} - \bar{X}_0|$ is obfuscated by fluctuations which are particularly significant for small N and which are due to the complicated dependence of the dynamics on N. In this paper we focus on the envelope of the graphs,

ignoring any transients for small N. The determination of the envelope is limited by the noise floor of the computation [Figs. 2(a-c)] as N increases. For example in Fig. 2(b), noise of magnitude e^{-10} dominates the measured value of $|\bar{a}-\bar{a}_0|$ for $N > 250$. The noise floor decreases slowly ($1/\sqrt{T}$), which requires exponentially increasing simulation times for extending the envelope to larger N.

The spacetime characteristics $\bar{X}$ for small ring networks is clearly different from the limiting characteristics $\bar{X}_0$ for larger network sizes despite the translational node symmetry inherent in ring networks. This reflects that a ring network below a certain network size does not behave as the sum of weakly interacting small ring networks, and deviations from microextensivity are apparent. The inverse of the envelope slope defines a length scale of interaction beyond which an STC system can be considered to be just a sum of its constituent parts. For the cGL system this length scale of interaction is decreasing with increasing parameter c_3 [Table I]. In general, envelope slope as well as length scale of interaction appear to be the same regardless of the variable X being measured, although the particulars of the fluctuations are slightly different. This is demonstrated in Figs. 2(b) and (c) for the GS ring network and four typical variables X, $X \in \{a, a^2, (da/dn)^2, r\}$ [34]; their length scale of interaction is 30 nodes [Table I].

The rapid convergence of $\bar{X} \to \bar{X}_0$ for large N suggests the conjecture that observations from a local region do not determine the size of a large STC ring network. This claim can be justified in terms of information transfer. The ring size is determined by observation of information that originates at the local region, travels around the ring, and finally reaches the local region again. For a ring network much larger than the length scale of interaction very little information will remain after a round trip, and the local region contains very little information about the ring size. Consequently, measures such as $\langle X_n\rangle$ (which, by symmetry, is typically equal to $\bar{X}$ for chaotic systems with periodic boundary conditions) must be constant over the range of sufficiently large system sizes.

In a *regular network with broken translational node symmetry due to no-flux boundary conditions* the local averages $\langle X_n\rangle$ near the boundaries do not match the spacetime average for a large ring network $\bar{X}_0$ [32]. Nodes that are sufficiently far away from the boundary on the other hand do not have access to information about the boundary and $\langle X_n\rangle \to \bar{X}_0$ as the distance from the boundary increases. The deviations $|\langle X_n\rangle - \bar{X}_0|$ decrease exponentially with the distance from the boundary for both systems (cGL, GS) and for a wide variety of variables X [Figs. 3(a-c)]. The sharp dips in $\ln|\langle X_n\rangle - \bar{X}_0|$ are due to zero-crossings of $\langle X_n\rangle - \bar{X}_0$ and occur at different nodes for different variables [35]. The comments about noise floor and fluctuations made in reference to Fig. 2 apply here as well.

The influence of a boundary condition rapidly diminishes as a function of distance from the boundary, since information about the presence of a boundary gets scrambled before it can be communicated with distant nodes. The inverse of the envelope slope defines a length scale of interaction below which an STC system depends on the boundary condition and reveals deviations from microextensivity. For the cGL system this length scale decreases with increasing parameter c_3 [Table I]. It is the same regardless of the variable X being measured (to within observational limits) as shown in Figs. 3(b) and (c) for

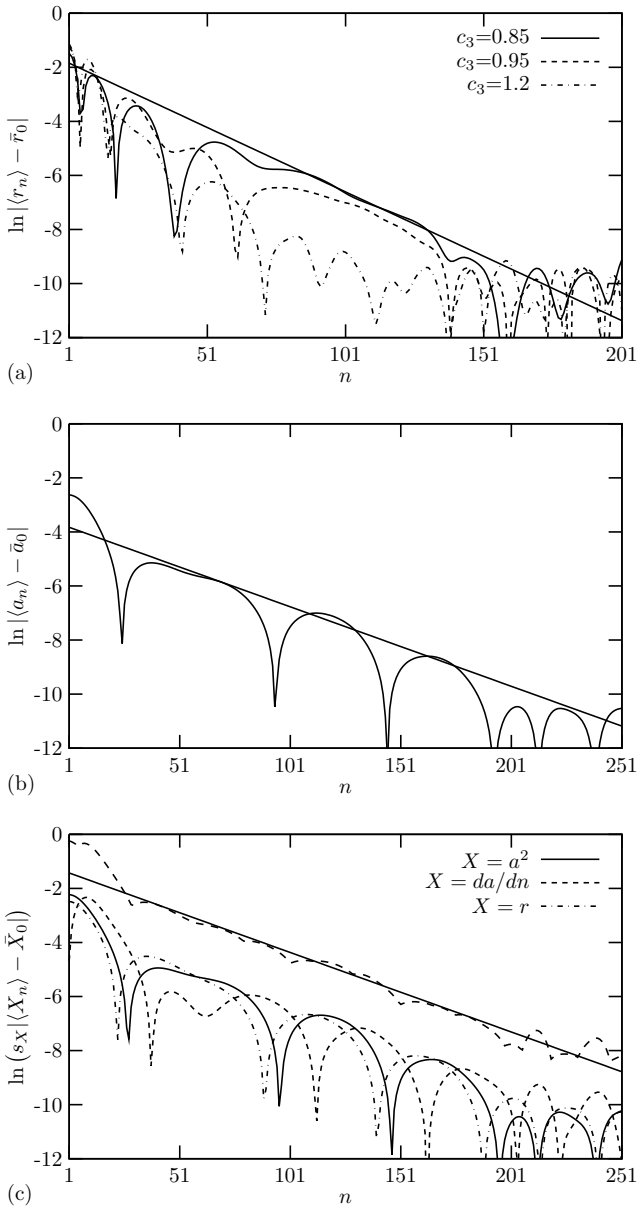

FIG. 3. Deviation of time averages [$\langle X_n\rangle$, Eq. (5)] from the spacetime average of a large ring network [$\bar{X}_0$, Eq. (7)] for varying nodes n near a no-flux boundary ($N = 1000$): (a) $\ln|\langle r_n\rangle - \bar{r}_0|$ for the cGL ring network ($c_1 = 3.5$, $c_3 \in \{0.85, 0.95, 1.2\}$) with $r = |z|$ the distance to the unstable focus; (b) $\ln|\langle a_n\rangle - \bar{a}_0|$ for the GS ring network ($\mu = 33.7$, $\Phi = 2.8$); (c) $\ln\left(s_X|\langle X_n\rangle - \bar{X}_0|\right)$ [35] for the same GS ring network as in (b) and different variables X ($X = a^2$, $X = da/dn$, and $X = r$ with r the distance to the unstable focus). s_X is a scale factor chosen to align all three traces vertically. The top trace corresponds to $\ln\left[\max_X\left(s_X|\langle X_n\rangle - \bar{X}_0|\right)\right]$; it is raised above the other traces for clarity. Envelopes of curves in (a) and (c) are fitted with a subjectively chosen linear function. The slope of the linear fit in (c) is shown in (b) for reference.

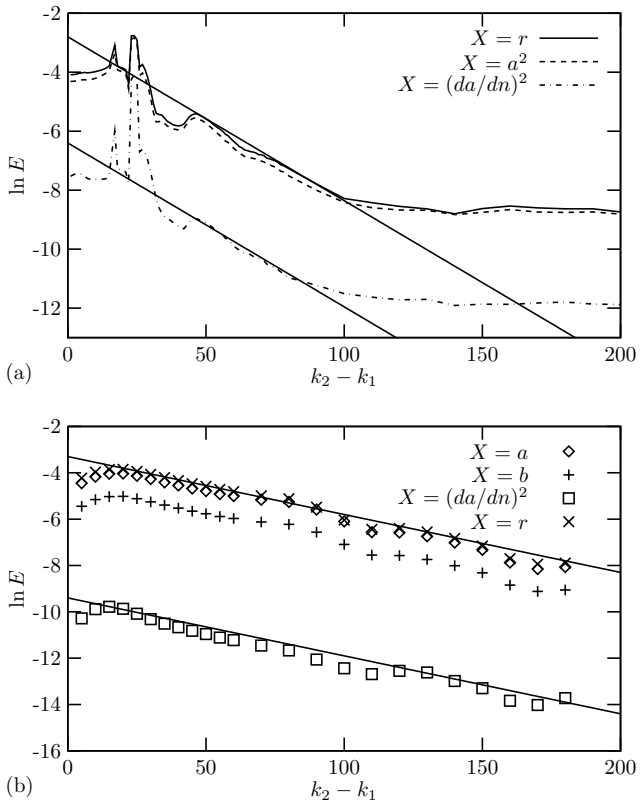

FIG. 4. Shortcut-induced deviations from microextensivity E [Eq. (9)] that are based on time averages $\langle X\rangle$ for varying shortcut lengths $k_2 - k_1$ in a ring network ($N = 1000$) with a single shortcut between node $k_1 = 1$ and k_2, for (a) the cGL system ($c_1 = 3.5$, $c_3 = 0.95$) and for (b) the GS system ($\mu = 33.7$, $\Phi = 2.8$). In each of the figures a subjectively chosen linear fit is determined and plotted twice (with the same slope) as a visual reference.

the case of a GS ring network and four typical variables X, $X \in \{a, a^2, da/dn, r\}$ [34]; the length scale of interaction is 34 nodes [Table I].

Nonlocal coupling (shortcut) between two network nodes also breaks the translational node symmetry within a ring network and affects the local dynamics. Local averages $\langle X_n\rangle$ near the two shortcut nodes differ from the spacetime average for a large ring network $\bar{X}_0$. Unlike in the case of the no-flux boundary, the nodes that are connected by the shortcut can be chosen. Consequently, varying the length of the shortcut within the ring network allows to measure the degree of interaction between the local disturbances surrounding each of the shortcut nodes.

To study the deviations of local dynamical characteristics in the presence of a single shortcut, we consider the reference case of a large ring network with a long shortcut between two nodes $k_1$and k_2 ($N = 2000$, and $k_2 - k_1 = 1000$); these nodes are separated by a distance much greater than the length scale of interaction. In this reference network, $X_n^s := \langle X_{k_1+n}\rangle$ denotes the average value of X for a node that is $|n|$ nodes away from the shortcut linkage k_1. Then the estimate X_n^e for the local average $\langle X_n\rangle$ at node n for a large ring network with a single shortcut of arbitrary length is given by

$$X_n^e - \bar{X}_0 = (X_{|n-k_1|}^s - \bar{X}_0) + (X_{|n-k_2|}^s - \bar{X}_0); \tag{8}$$

it depends on data X_i^S of the reference ring network with a long shortcut. This estimate is trivially fulfilled if the local characteristics is measured at a node n clearly away from both linkages k_i, i.e. $|k_i - n|$ much larger than the length scale of interaction, since then $X_i^s \approx \bar{X}_0$ in Eq. (8). If the local characteristic is measured at a location n that is within the interaction length scale of at least one of the linkages, then at least one of the differences $X_{|n-k_i|}^s - \bar{X}_0$ in Eq. (8) is nonzero, and the estimate represents a linear superposition of local characteristics. Eq. (8) is used to determine shortcut-induced deviations from linearly additive behavior (E) expressed as the RMS error between the estimate X_n^e and the true local average $\langle X_n\rangle$ at node n,

$$E = \sqrt{N^{-1}\sum_{n=1}^{N}(X_n^e - \langle X_n\rangle)^2}. \tag{9}$$

The logarithmic variation of the RMS error E with the shortcut length $k_2 - k_1$ is plotted in Fig. 4 for the cGL system (a) and the GS system (b) using different variables X. Only a few variables X were available for the cGL system, because the $U(1)$ symmetry of the dynamical equation leads to $\left\langle A_n^p\right\rangle = \left\langle B_n^p\right\rangle$ for even powers p and $\left\langle A_n^p\right\rangle = \left\langle B_n^p\right\rangle = 0$ for odd powers. In all cases E approaches zero for large shortcut lengths. This is expected since the local regions around the two linkages do not interact for long shortcuts, the linear superposition in the estimate is valid, and the ring network behaves as a sum of its parts in the presence of a long shortcut. This is similar to the case of no-flux boundary conditions in Fig. 3 where the deviations from extensivity also vanish for increasing distance from the boundary condition. For smaller shortcuts however, E does not vanish, which indicates that the two local regions centered at the linkages do interact to cause deviations from microextensivity. In both systems there is an exponential decay of E with increasing shortcut length. The length scale of the decay is independent of the variable X within observational accuracy [Fig. 4, Table I].

The measure E was designed to quantify shortcut-induced deviations from microextensivity. E determines the degree to which the local regions near the linkages of the shortcut interact dynamically with each other in a nonlinear way. It determines how far apart the nonhomogeneous nodes (linkages) of a network need to be in order for the network to be extensive; a nonzero E represents the degree to which the network is not simply a linear sum of its parts.

In this section we have quantified the length scale of interaction with long-time averages of various variables X. The variables however fluctuate in time, as does the nature of the local dynamics; long-time averages span over many temporally local artifacts. For example, STC in the GS system exhibits an irregular distribution of *local extinctions* where neighboring trajectories approach the stable steady state of the uncoupled system ($a = 1$ and $b = 0$). These local extinctions are quickly erased by an excitation wave that travels inwards

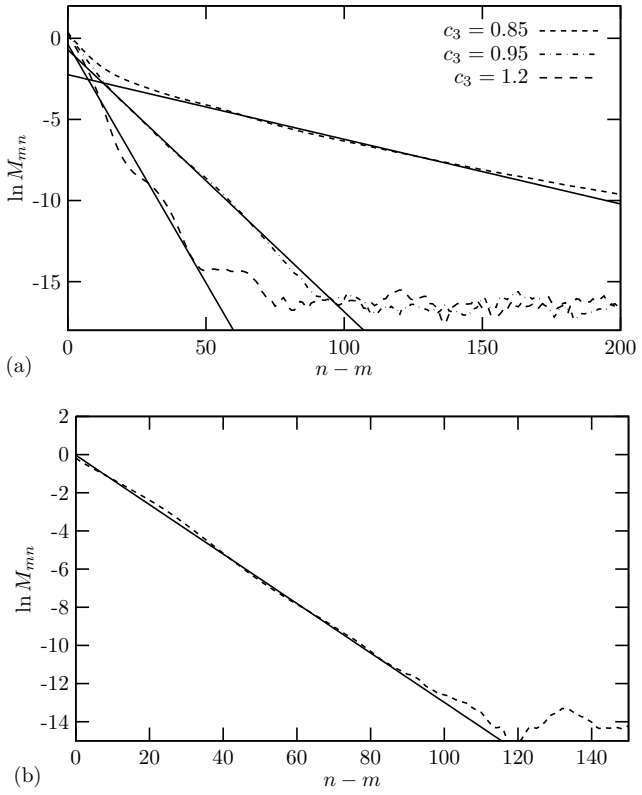

FIG. 5. Logarithm of same-time mutual information M_{mn} vs. node separation $|n - m|$ for (a) the variable a of the cGL ring network ($c_1 = 3.5$) and for (b) the variable a of the GS ring network ($\mu = 33.7$, $\Phi = 2.8$). For variable r the deviations from the linear trend were more pronounced. Each curve was approximated with a least-squares linear fit for the largest range of node separations $|n - m|$ with an approximately linear relation. The probabilities were computed from histograms with 5 bins for each variable, so 25 bins for the joint probability $p(X_m, X_n)$.

from both sides [white triangular structures in Fig. 1(b)]. Such an excitation wave carries the information (without loss) that the local extinction is not a global extinction [36], since an excitation wave cannot be present in the case of a global extinction. Local extinctions occur with a frequency that diminishes exponentially with their width, so the range of information transfer by excitation waves due to local extinctions is limited; small extinctions don't have long range and large extinctions are very rare and not statistically significant.

IV. MEASURING INFORMATION TRANSFER VELOCITY

Although the characterization of a length scale of interaction via node averages (Sect. III) does not involve information theoretic concepts, the detectability of a boundary condition by a node that is some distance from the boundary necessarily involves transmission of information. In this section we examine the flow of information through a reaction-diffusion network.

The mutual information quantifies the amount of information about an observable shared between two nodes, or more specifically the amount of information that can be learned about the variable X at node m through observation of variable X at node n. The *mutual information* M_{mn} between nodes m and n as observed through variable X is defined as

$$M_{mn} = \sum_{X_m, X_n} p(X_m, X_n) \ln \frac{p(X_m, X_n)}{p(X_m)p(X_n)}. \qquad (10)$$

$p(X_m)$ and $p(X_n)$ are the marginal probabilities and $p(X_m, X_n)$ is the joint probability associated with the pair of measurements X_m and X_n of observable X at nodes m and n. The probabilities were computed from histograms with 100 bins for each variable, so 100^2 bins for the joint probability $p(X_m, X_n)$. In this case the noise floor, which is a function of simulation time and number of histogram bins, is too large and limits the range of $|n - m|$ with usable values of M_{mn}. A reduction to 5 bins per variable sufficiently decreases the noise floor (Figs 5).

For the cGL as well as the GS system the logarithm of the mutual information $\ln M_{mn}$ decays rather linearly with node separation $|n - m|$, until it flattens due to the noise floor [Figs. 5(a) and (b)]. The length scales associated with the least-squares linear fit are listed in Table I. It is clear that the length scales (inverse slopes) associated with $\ln M_{mn}$ vs. $|n-m|$ (Fig. 5) are not equal to those associated with node averages, $\ln|\bar{X} - \bar{X}_0|$ vs. N (Fig. 2) or $|\langle R_n\rangle - \bar{R}_0|$ vs. n (Fig. 3), but they are equal to each other within an order of magnitude. The length scales associated with mutual information show much greater variation across the various parameter values of c_3 in the cGL system than do the length scales associated with the other measures (Table I).

Mutual information is similar to the temporal node averages from Sect. III in that both describe the ability of the network to communicate across distances. There are however important differences between temporal node averages and mutual information. Mutual information is measured by comparing two nodes to each other and node averages involve measurement of individual nodes. Mutual information can therefore be applied to a homogeneous network with fixed size, when temporal node averages would be constant across the nodes and thus obscure the information flow within the system. Node averages on the other hand measure the characteristics of individual parts of a system to identify unusual node characteristics (such as near a no-flux boundary).

Mutual information defines a length scale over which a system becomes decorrelated; a temporal consideration must be added to characterize information flow. One option is to introduce a delay in the measurement of one of the nodes, so that a measurement $X_m(t)$ is compared with $X_n(t+\Delta t)$ for some delay time Δt. For a given pair (m, n), the delayed mutual information should reach a first local maximum at some delay Δt. If Δt is proportional to the node separation $|n - m|$ for a range of $|n - m|$ values, their ratio defines an information velocity, $v = |n - m|/\Delta t$. Time delayed mutual information, however, does not distinguish between information traveling from one node to the other versus information reaching the two nodes from a source external to them. For spatiotemporal chaos in the cGL and GS system delayed mutual information did not qualify to define a (constant) information velocity.

		cGL: $c_3 = 0.85$	cGL: $c_3 = 0.95$	cGL: $c_3 = 1.2$	GS
Decay of $\lvert\bar{X} - \bar{X}_0\rvert$	Fig. 2	67	28	24	30
Decay of $\lvert\langle X_n\rangle - \bar{X}_0\rvert$	Fig. 3	21	19	11	34
Decay of E	Fig. 4	-	18	-	40
Decay of M_{mn}	Fig. 5	25.1	6.19	3.40	7.72
Decay of $\lvert D_{\mathcal{L}} - N/\xi_\delta\rvert$		n/a	31.2 [37]	32.5 [37]	n/a
Chaotic length scale ξ_δ	Eq. (4)	10.7 [37]	8.7 [37]	6.7 [37]	16.3 [20]
Lyapunov dimension density $\lim_{N\to\infty} \Sigma^+/N$		-	-	-	0.001126 [20]
Information transfer velocity v	Eq. (13)	-	4.2	-	3.3

TABLE I. Length scales of the exponential decay (in units of number of nodes) for various measures applied to the complex Ginzburg-Landau (cGL) network ($D = 4$, $c_1 = 3.5$) and to the Gray-Scott (GS) network ($D = 16$, $\mu = 33.7$, $\phi = 2.8$). The chaotic length scale ξ_δ [nodes] is added for comparison. The Lyapunov dimension density [nats/(node·time)] and information transfer velocity [nodes/time] are used in Sect. V. Cells marked "-" were not computed; no significant deviation from microextensivity in $D_{\mathcal{L}}$ exists for cells marked "n/a." $\lvert D_{\mathcal{L}} - N/\xi_\delta\rvert$ refers to deviation from extensivity of Lyapunov dimension.

Schreiber has proposed to study information flow via transfer entropy [14]. The *transfer entropy* $T_{\Delta n\Delta t}$ describes the amount of information that is revealed about node $n + \Delta n$ at time $t + \Delta t$ by measurement of a node n at time t and at earlier times $t - 1, t - 2, \ldots$, but that is not available from measurements of node $n + \Delta n$ at times previous to $t + \Delta t$ ($t + \Delta t - 1$, $t + \Delta t - 2, \ldots$). Due to memory constraints, we only used a single sample at node n (i.e. only the sample at time t) and a single historical sample at node $n + \Delta n$ (i.e. the subject sample at time $t + \Delta t$ and the historical sample at time $t + \Delta t - u$ for a constant value u). In this case, the equation for Schreiber's transfer entropy reduces to

$$T_{\Delta n\Delta t} = \sum_{A,B,C} p(A,B,C) \ln \frac{p(B|A,C)}{p(B|C)}, \tag{11}$$

with

$$\begin{aligned} A &= X_n(t), \\ B &= X_{n+\Delta n}(t + \Delta t), \text{ and} \\ C &= X_{n+\Delta n}(t + \Delta t - u). \end{aligned} \tag{12}$$

Δn is the spacing between the two nodes, Δt is the transfer time delay, and u is the historical time delay for node $n + \Delta n$. $p(B|C)$ is the conditional probability of measurement B conditioned on measurement C and $p(B|A,C)$ is the conditional probability of measurement B conditioned on measurements A and B.

Transfer entropy measures the flow of information through a system, and as such requires an entropy source. Any system with a positive Lyapunov exponent spontaneously creates entropy; however, we introduce an additional source of entropy at node n by adding a unidirectional shortcut between node n and another node m that is far away from n ($|n - m| = N/2$) so that entropy produced in a remote part of the system gets fed into node n. Specifically, an extra diffusion path $\delta_{in}(\delta_{jm} - \delta_{jn})$ is added to the Laplacian term Δ_{ij} in Eq. (1). This additional source of entropy greatly enhances the effectiveness of the algorithm to determine information velocities.

For the observable X in Eq. (12) we have used the angle of the trajectory in phase space in relation to the unstable focus, as measured from the $\hat{a}$ direction. This observable has a clearly defined range ($-\pi$ to π) and is uniformly distributed in the case of the cGL system and rather evenly distributed in the case of the GS system; these characteristics lead to efficient usage of histogram bins. The probabilities in Eq. (11) were computed from histograms for X with 30 bins; the joint probabilities $p(A,B,C)$ are accumulated into 30^3 bins. The historical time delay u was chosen somewhat arbitrarily as $u = 8$ for the cGL system and $u = 2.4$ for the GS system; these values are large enough to allow evolution of the system (so that B and C will often be in different histogram bins) but small enough that measurement C still has predictive relevance regarding measurement B.

For a range of Δn the transfer entropy $T_{\Delta n\Delta t}$ was calculated as a function of the transfer time delay Δt; the graphs exhibit a peak for a positive value of Δt with the maximum value decreasing with increasing distance Δn to node n (Fig. 6). The spatial progression of the maximum (increasing Δn) depends in good approximation linearly on its transfer delay time for the two cases tested, which justifies the definition of an *information transfer velocity*,

$$v = \Delta n/\Delta t. \tag{13}$$

Due to complications caused by the extraneous oscillations of $T_{\Delta n\Delta t}$, the value of v was chosen subjectively, $v = 4.2$ for the cGL system and $v = 3.3$ for the GS system. Figure 6 shows the variation of the transfer entropy with the time delay Δt for the cGL system and the GS system, corrected by the information velocity term to align the graphs for different Δn. The peaks align with some relatively small deviations, which confirms the existence of an information transfer velocity according to $\Delta t = \Delta n/v$. For the GS system there is an anomalous shift in the peak towards larger values of Δt at around $\Delta n = 70$.

In the absence of the additional entropy source in the form of a unidirectional shortcut, the peaks of $T_{\Delta n\Delta t}$ are less well defined, although the correction with the information transfer velocity still yields an approximate alignment of the graphs. Using delayed mutual information rather than $T_{\Delta n\Delta t}$ we get similar results. In the presence of the unidirectional shortcut, the transfer entropy propagates with an approximately constant velocity for nodes within some distance Δn from node n in both systems. Without the shortcut we find an approximate alignment for small Δn of less well defined peaks for the cGL

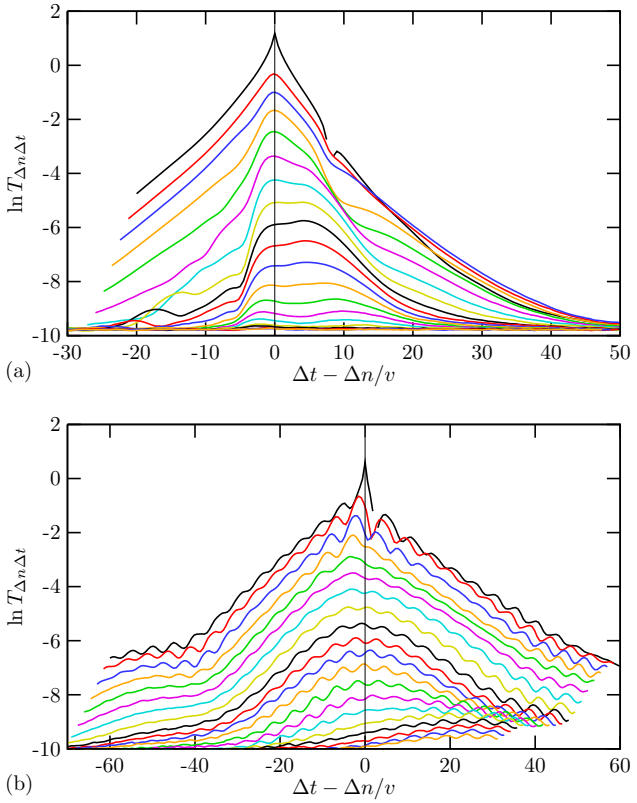

FIG. 6. (Color online) Logarithm of transfer entropy $T_{\Delta n \Delta t}$ vs. time delay Δt for a variety of node spacings Δn ($\Delta n = 0, 5, 10, 15$, etc. from top to bottom) for (a) the cGL ring network ($c_1 = 3.5$, $c_3 = 0.95$) and for (b) the GS ring network ($\mu = 33.7$, $\Phi = 2.8$). Each curve is shifted in Δt using the estimated information transfer velocity v ($v = 4.2$ for cGL system, and $v = 3.3$ for GS system) to allow the peaks to align. The break in the graphs at $\Delta n = 0$, $\Delta t = u$ occurs because $T_{\Delta n \Delta t} = 0$ at that point [Eqs. (11-12)]. The location m of the additional entropy source is at $|n - m| = N/2$ with $N = 1000$ the network size.

ring network, and no alignment for the GS ring network. For both information measures we find that the addition of an additional entropy source clearly helps to determine the velocity of the particular information flow.

The presence of an abnormal node (boundaries or shortcuts) is a piece of information, and it takes time for this information to travel to a remote area. The spatial localization of unusual node characteristics due to boundary conditions and abnormal network topology (e.g. shortcuts) as described in Sect. III can be interpreted as information being attenuated as it travels away from the abnormal nodes to neighboring nodes. The limited spatial reach of this information is conjectured to be related to the amount of time required for information to travel from one region to another. Information transfer velocity could then transform any of the length scales L defined in this paper into characteristic time scales T for information attenuation ($T = L/v$).

V. MEASURING SPACE-TIME INFORMATION FLOW WITH FINITE PERTURBATIONS

The spatially limited influence of boundary conditions defines various length scales of interaction (Sect. III). Finite dynamical perturbations give insight into the spatiotemporal information flow. Spatiotemporal chaos is exposed to a spatially localized and temporally periodic perturbation. The perturbation is added in Eq. (1), yielding

$$\frac{d\mathbf{x}_n}{dt} = \mathbf{F}(\mathbf{x}_n) + DH \sum_{j=1}^{N} \Delta_{nj} \mathbf{x}_j + p(t)\mathbf{q}(n), \tag{14}$$

where p is localized in time and periodic with period P, and $\mathbf{q}$ is localized in space. In the interest of numerical stability, p and $\mathbf{q}$ were chosen to be bump functions,

$$p(t) = f\left(2[(t \bmod P)/w_t] - 1\right) \tag{15}$$

$$\mathbf{q}(n) = \mathbf{q}_0 f\left([n - n_0]/w_n\right), \tag{16}$$

with

$$f(\alpha) = \begin{cases} exp\left(1 - \frac{1}{1-\alpha^2}\right) & \text{if } |\alpha| < 1 \\ 0 & \text{otherwise.} \end{cases} \tag{17}$$

w_t refers to the duration of the perturbation; it needs to be long enough to have a measurable effect on the system's information flow. P is the period between successive perturbations; it needs to be large enough for the system to reach its natural state before the next perturbation, $w_t << P$. The perturbation of radius w_n is centered at the node $n_0 = N/2$; it must be wide enough such that the perturbation is not immediately dampened by diffusion. $w_n = 10$, $w_t = 1$, $P = 50$ for the cGL system, and $P = 300$ for the GS system were chosen in this paper. $\mathbf{q}_0$ determines the direction and amplitude of the perturbation; we used $\mathbf{q}_0 = (5, 0)$ for the cGL system, and $\mathbf{q}_0 = (2, 0)$ for the GS system.

The consequences of the periodic perturbations for the local characteristics of the dynamical variable X at a time τ after the onset of each perturbative event are quantified via averages $\langle X_{n\tau} \rangle$,

$$\langle X_{n\tau} \rangle = \lim_{K \to \infty} \frac{1}{K} \sum_{k=1}^{K} X_n(t = kP + \tau), \tag{18}$$

where n and τ ($0 \leq \tau < P$) represent the spatial and temporal indices.

Figure 7 shows the spatiotemporal deviations of $\langle X_{n\tau} \rangle$ from the large-ring baseline average $\bar{X}_0$ for the cGL ring network and the GS ring network. The spatially and temporally localized perturbations clearly affect the dynamical characteristics in the space-time neighborhood of the perturbation. The pseudorandom structure filling the background of the plots presents the noise floor, which decreases logarithmically as a function of simulation time. The dotted lines in Fig. 7 have

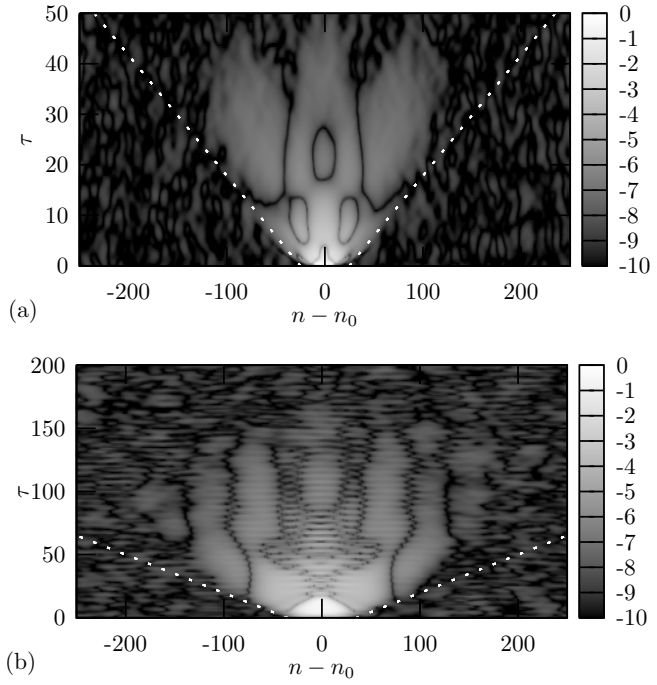

FIG. 7. Spatiotemporal deviations in the average nodal characteristics for perturbed [Eq. (14)] and unperturbed [Eq. (1)] network dynamics at node n and at a time τ after the onset of the perturbation. (a) $\ln|\langle r_{n\tau}\rangle - \bar{r}_0|$ for the cGL ring network ($c_1 = 3.5$, $c_3 = 0.95$, $N = 500$, $P = 50$, $\mathbf{q}_0 = (5, 0)$, and $K = 7.2 \times 10^6$), and (b) $\ln|\langle a_{n\tau}\rangle - \bar{a}_0|$ for the GS ring network ($\mu = 33.7$, $\Phi = 2.8$, $N = 500$, $P = 300$, $\mathbf{q}_0 = (2, 0)$, and $K = 6.0 \times 10^5$). The other parameters for the spatiotemporally localized finite perturbation are $n_0 = N/2$, $w_n = 10$, and $w_t = 1$. The dotted lines have slope equal to the information transfer velocity [Eq. (13)] and are plotted for comparison.

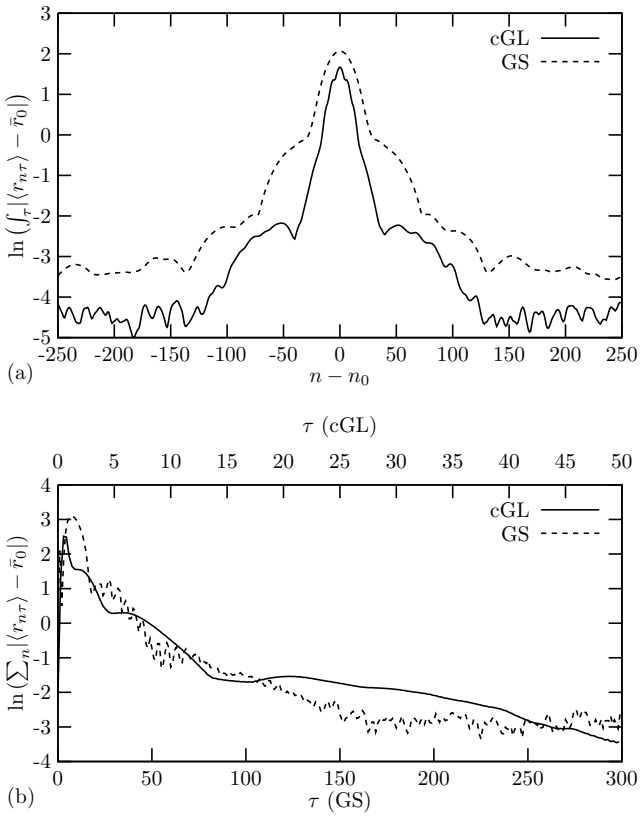

FIG. 8. (a) The data from Fig. 7, collapsed along the temporal (τ) axis. (b) The data from Fig. 7, collapsed along the spatial (n) axis. Note that the time axis is scaled differently for the cGL and GS traces.

a slope equal to the information transfer velocity [Eq. (13)]; these lines closely match the perturbation wavefront. On the one hand this is to be expected since the perturbation can be considered as a piece of information that travels through the system. On the other hand, the connection between information transfer velocity and the perturbation wavefronts in Fig. 7 is not trivial. Information transfer velocity is defined in terms of information theoretic quantities [Eq. (11)] and based on a passive measurement of the dynamical system, whereas the perturbation front is defined by a nodal average [Eq. (18)] and measured by actively perturbing the dynamical system.

Information on injected signals (Fig. 7) as well as information on boundary conditions (Fig. 3) cannot travel across great distances through a medium (network) of STC in the case of the cGL network and the GS network. A sender could encode a message into the perturbation term $p(t)\mathbf{q}(n)$ of Eq. (14) to be sent through the reaction-diffusion network. Due to the scrambling of information a receiver sufficiently far from the sender could not observe any effect even after integrating over millions of transmissions [$K = 7.2 \times 10^6$ in Fig. 7(a)]. In analogy a boundary condition (shortcut) can be considered to be a sender of the message "presence of a boundary condition (shortcut)," and a far away receiver is not able to detect this signal.

The temporal or spatial reach of the finite size perturbation follows from the deviation $|\langle X_{n\tau}\rangle - \bar{X}_0|$ by summation over either the n or the τ parameter. The nodal deviations $\int_\tau |\langle X_{n\tau}\rangle - \bar{X}_0|$ in Fig. 8(a) show a clear decrease with distance to the perturbation. Whether this decay is exponential with the distance $|n - n_0|$ to the perturbation is not clear; longer simulations are necessary to reduce the noise floor, although lowering the noise floor requires exponentially longer simulation times. The current simulation times exceeded 10^8 time units. In case there is an exponential decay the decay coefficient would provide another candidate for the length scale of interaction. The temporal reach $\sum_n |\langle X_{n\tau}\rangle - \bar{X}_0|$ of the spatiotemporal perturbations across the entire network decays with the time distance (τ) to the onset of a perturbation [Fig. 8(b)]. It is again not clear whether this decay is exponential; it appears that there is a transition from a fast decay rate for small τ to a slower decay rate for larger τ. The decay rate provides a measure of how fast the system recovers from finite size perturbations.

The attenuation of deviations $\sum_n |\langle X_{n\tau}\rangle - \bar{X}_0|$ over time τ can be explained in terms of the Kolmogorov-Sinai entropy, but the attenuation rate is clearly underestimated. Chaotic systems have positive Lyapunov exponents and so they spontaneously create information; the stretching process magnifies pieces of information that were previously unobservable. The average rate of information production is given by the

Kolmogorov-Sinai entropy, which is bounded from above by the sum of positive Lyapunov exponents, Σ^+ [39]. Because a system has a maximum capacity of information that depends on the resolution and the accuracy of the measurement, as information is created other information must be destroyed [40]. Therefore, the Kolmogorov-Sinai entropy (approximated by Σ^+) provides an estimate for the rate of information loss. We compare the Kolmogorov-Sinai entropy with the attenuation rate of $\sum_n |\langle X_{n\tau}\rangle - \bar{X}_0|$ with τ in Fig. 8(b). For the GS ring network the Kolmogorov-Sinai entropy density (approximated by the slope of Σ^+ vs. N in [20]) is 0.001126 nats/(node·time). The perturbation spreads out to an area less than 300 nodes (Fig. 8(b)), which yields an entropy less than 0.34 nats/time in this region. The inverse gives a characteristic time for information loss greater than 3.0. In contrast, the decay constant for $\sum_n |\langle a_{n\tau}\rangle - \bar{a}_0|$ in Fig. 8(b) is somewhere in the range of 12 to 56 depending on which part of the graph is considered. This shows that our calculation clearly underestimates the time of recovery from a finite perturbation.

For the ring network in Fig. 7 the message sent by the localized perturbation is fully attenuated before it can complete the loop around the ring. In this case the ring network is large enough so that the information propagating in both directions around the ring network is completely scrambled before the propagation fronts meet; a local portion of the network is then unable to communicate with itself across the ring, i.e. the network is unable to "detect" its own size, and microextensivity should be guaranteed. In contrast, if the ring network is smaller (e.g. $N = 100$ or 200) there would be interference between the right moving and left moving information fronts; the size of the ring is detectable, and deviations from microextensivity are expected. We further argue that even if information is spontaneously generated from only within a system, like for example the local extinct regions in the GS system, the spatial extent of their influence is still governed by the results in this chapter (Fig. 7). Consequently, the size of a ring network is only detectable for small systems even in the absence of external perturbations.

VI. LENGTH SCALE OF INTERACTION IN A SYSTEM WITH STABLE CHAOS

We present preliminary results to show that the various length scales of interaction introduced in the previous chapters also apply to the phenomenon of *stable chaos* [41, 42], an irregular spatiotemporal dynamics with negative Lyapunov exponent. Stable chaos is additionally characterized by disordered spatial structures (finite correlation dimension), exponentially decaying temporal and spatial correlations, and a finite lifetime that increases exponentially with the size of the system, a property shared by the Gray-Scott system and other transient spatiotemporally chaotic systems. Stable chaos is

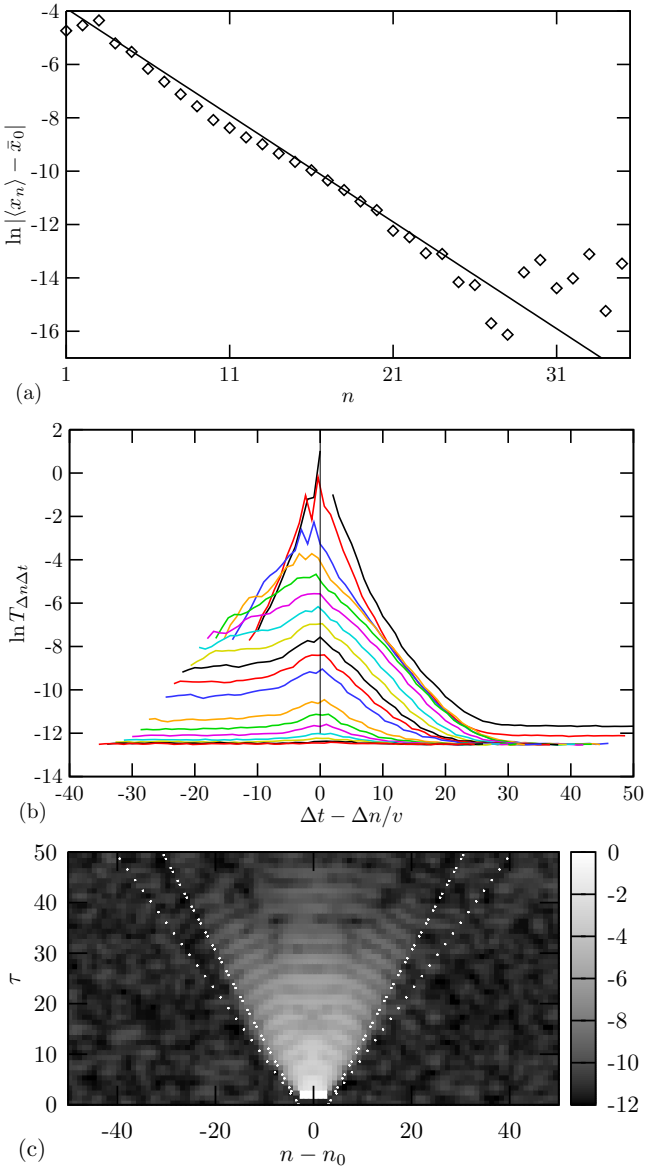

FIG. 9. (Color online) Length scales of interaction for stable chaos in the coupled map lattice [Eq. (19) with $a = 0.07$, $b = 2.7$, $c = 0.1$, and $\epsilon = 2/3$]. (a) Deviation of time averages [$\langle x_n\rangle$, Eq. (5)] from the spacetime average of a large ring network [$\bar{x}_0$, Eq. (7)] for varying nodes n near a no-flux boundary ($N = 1000$), in analogy to Fig. 3. (b) Logarithm of transfer entropy $T_{\Delta n \Delta t}$ vs. time delay Δt for a variety of node spacings Δn ($\Delta n = 0, 1, 2, 3$, etc. from top to bottom), in analogy to Fig. 6. Each curve is shifted in Δt using the estimated information transfer velocity v ($v = 0.75$ nodes/timestep) to allow the peaks to align. (c) Spatiotemporal deviations in the average nodal characteristics for perturbed [Eq. (14)] and unperturbed [Eq. (19)] network dynamics at node n and at a time τ after the onset of the perturbation, $\ln|\langle x_{n\tau}\rangle - \bar{x}_0|$, (with parameters $N = 200$, $P = 100$, $n_0 = N/2$, $q_0 = 1$, $K = 1.3 \times 10^8$, $w_n = 3$, and $w_t = 2$ [43]), in analogy to Fig. 7. The dotted lines have slope equal to the information transfer velocity v [Eq. (13)], and the double dotted lines have slope equal to the disturbance propagation velocity v_d in Eq. (20).

often studied in the following coupled map lattice (CML),

$$x_n(t+1) = \frac{\epsilon}{2} f(x_{i-1}(t)) + (1-\epsilon) f(x_i(t)) + \frac{\epsilon}{2} f(x_{i+1}(t)),$$
$$f(x) = \begin{cases} bx & \text{if } 0 < x < 1/b \\ a + c(x - 1/b) & \text{if } 1/b \leq x < 1, \end{cases} \quad (19)$$

where time t is discrete and n refers to the node number. We use the same parameters as in [41], i.e. $a = 0.07$, $b = 2.7$, $c = 0.1$, and $\epsilon = 2/3$, for which the system reaches an asymptotically periodic state after a transient time.

We show that the techniques set forth in this paper apply equally well to determining length scales of interaction in this stable chaotic CML. Figure 9(a) shows an exponential decrease of the deviation of time averages $\langle x_n \rangle$ near a no-flux boundary condition as compared to the spacetime average of a large ring network $\bar{x}_0$, using the technique outlined in Sect. III. The linear fit gives a short characteristic length scale of 2.5 nodes. Figure 9(b) shows the transfer entropy $T_{\Delta n \Delta t}$ for this CML, using the technique outlined in Sect. IV. It is not clear *a priori* that this measure provides a useful result in the case of stable chaos; the negative Lyapunov exponent relates to a zero Kolmogorov-Sinai entropy, and therefore a vanishing local information production rate. Nevertheless the sequence of transfer entropies in Fig. 9(b) defines an information transfer velocity [Eq. 13], similar to the chaotic and transient chaotic system in Fig. 6. The information transfer velocity is approximately 0.75 nodes/timestep.

An alternate measure of velocity was defined in [41] via the propagation of disturbances. A localized perturbation is applied to one of a pair of identical systems, and the radius of the region (range of nodes) $d(t)$ for which the two systems differ by more than a small tolerance is measured. The disturbance propagation velocity v_d is then defined as

$$v_d = \lim_{t \to \infty} \frac{\langle d(t) \rangle}{t}, \quad (20)$$

where $\langle \cdot \rangle$ represents an average over several simulations. We compute $v_d = 0.557 \pm 0.004$ nodes/timestep for a tolerance of 10^{-3} and an average over 100 simulations.

Figure 9(c) shows the average spatiotemporal response to a localized perturbation using the technique of Sect. V. The information transfer velocity ($v = 0.75$ nodes/timestep, single-dotted line) provides a good match for the propagation wave front for small times τ, and the disturbance propagation velocity ($v_d = 0.557$ nodes/timestep, double-dotted line) fits well for later times τ.

As demonstrated in Figs. 9(a)-9(c) stable chaos in this CML behaves similar to the asymptotic and the transient spatiotemporally chaotic systems; information is attenuated as it travels through the system and remote parts become essentially independent of each other. The negative Lyapunov exponent in stable chaos provides an interesting perspective to the discussion in Sect. V; the Kolmogorov-Sinai entropy is zero and yet information is attenuated. In this case there must be more going on than new information pushing out old information [40]. The negative Lyapunov exponent results in quenching tiny perturbations, and thus in removing information, but the analysis for large perturbations is more complicated.

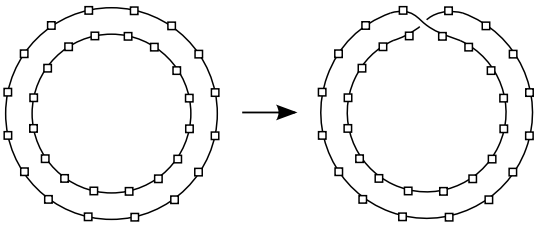

FIG. 10. A transformation that turns two ring networks each having N nodes into one network with $2N$ nodes, without changing the local network structure or the total number of nodes.

VII. DISCUSSION

In this paper we have put forth a variety of characteristic length scales of interaction in reaction-diffusion networks, applying them to spatiotemporal chaos (STC) in the complex Ginzburg Landau (cGL) network, to transient spatiotemporal chaos in the Gray-Scott (GS) network, and to stable chaos in a coupled map lattice. Each of these length scales relates to the localization of observable phenomena. Beyond the length scale associated with space time averages $|\bar{X} - \bar{X}_0|$ for variable X (Fig. 2) the specific size of a ring network begins to become insignificant. Effects of boundary conditions become insignificant for nodes that are far from the boundary in comparison to the length scale associated with nodal average $|\langle X_n \rangle - \bar{X}_0|$ (Fig. 3). Interactions between regions with special network topologies (e.g. diffusion shortcuts between distant nodes) become insignificant if the regions are separated by a distance that is large in comparison to the length scale associated with E (Fig. 4). These length scales are listed in Table I together with the chaotic length scale ξ_δ [1] [Eq. (4)] and the length scale based on mutual information (Fig. 5). They are in general not proportional to each other, except that ξ_δ is close to twice the length scale associated with $|\langle X_n \rangle - \bar{X}_0|$. Further studies would reveal whether this is significant or just a coincidence.

These various length scales of interaction are of practical importance for Ruelle's concept of extensivity [15]. Suppose two identical ring networks each contain N nodes and each have Lyapunov dimension $D_\mathcal{L}$, so that the composite system (the set product of both rings) has Lyapunov dimension $2D_\mathcal{L}$. Suppose that the two rings are joined together to create a single ring network with $2N$ nodes (Fig. 10). If the Lyapunov dimension for the transformed ring network ($2N$ nodes) is $2D_\mathcal{L}$, the system is extensive [1, 16]. Sect. III demonstrates that such a transformation has no impact on node averages $\langle X_n \rangle$ for a wide range of variables X if the ring networks are large enough. Although there is no formal connection between Lyapunov dimension and nodal average $\langle X_n \rangle$, it seems reasonable that any change in the support and natural measure of a chaotic attractor that changes its dimension $D_\mathcal{L}$ would also impact $\langle X_n \rangle$ for some variable X. Similarly, the length of a shortcut should have no impact on Lyapunov dimension as long as the shortcut is much longer than the length scale associated with E (Fig. 4).

The independence of local dynamics on system size (as

measured in Sect. III) for large enough systems should guarantee microextensivity for large systems. According to Ruelle extensive systems have no long scale correlations and behave as a sum of their parts [15]. This implies that the Lyapunov dimension density could be calculated through the observation of local regions of an STC system. Although such a method is not yet known, it can be assumed that any change of Lyapunov dimension density (for certain network sizes) would necessarily require some observable change in local dynamics. Or in other words, if the total network size has no observable effects on the local dynamics for large systems, the Lyapunov dimension density should be constant as well. This hypothesis is supported by the results of Fishman and Egolf [25] who showed that the cGL system exhibits significant deviations from microextensivity in Lyapunov dimension for small system sizes: the magnitude of these deviations decreases exponentially with the size of the system [25]. We have calculated the length scale associated with the exponential decay of these deviations from extensivity; they are printed in Table I [37]. The length scales are about 30 nodes for the two cGL networks where deviations were found.

Recently Karimi and Paul have reported deviations from microextensivity in the Lorenz-96 model [44] that do not diminish with system size. The Lorenz-96 model differs from the cGL and GS models in that the coupling between adjacent nodes is nonlinear and not Laplacian. In addition the spatiotemporal patterns appear to be approximately spatially periodic even in the chaotic regime, in contrast to the (apparent) lack of large scale structures in the cGL and GS patterns. This may indicate that in the Lorenz-96 model the deviations from microextensivity persist for truly large sizes. In this case the techniques outlined in this paper may reveal large scrambling length scales such that a boundary condition (Sect. III) or a finite perturbation (Sect. V) could be observable far from its source. The effect of boundary conditions on defect chaos in the two-dimensional cGL system was studied by Eguiluz et al [45]. This might be another case with possibly long interaction length scales as topological defects are conserved and can only be created at the boundary; this is to be explored in further studies.

Oscillatory deviations from extensivity that diminish with network size have also been reported in the Wacker-Schöll system for the logarithm of the average lifetime of transient spatiotemporal chaos [20]. In this system spatiotemporal chaos typically collapses into a spatiotemporally periodic state, with certain spatial periods accessible to certain system sizes (system sizes that are close to a multiple of the spatial period) [20]. The resulting deviations from extensivity and their decrease with network size [20] are expected to have little in common with the deviations reported in [25] and in this paper; this paper concerns measurements made on the chaotic saddle (GS system) or on the chaotic attractor (cGL system) whereas transient lifetime becomes manifest only when a system exits from a chaotic saddle.

Spacetime averages $\bar{X}$ for a small ring network differ significantly from the limiting case $\bar{X}_0$ for large networks (Fig. 2). Thus any type of measurement on small networks can be considered an anomaly. This is relevant for determining e.g. the average lifetime of transient spatiotemporal chaos, which typically increases exponentially with network size [5, 8, 9, 18, 20] in the range of network sizes that are currently computationally accessible (even with supercomputing power). For the GS-ring network we can barely reach the range for which network sizes do not matter anymore [20], where $\bar{X}$ approaches its limit $\bar{X}_0$ ($N \approx 200$ in Fig. 2). Therefore it is currently not clear whether this exponential dependence reported widely in the literature will still hold for large enough networks, or if so what value the slope of log-lifetime vs. N will take as $N \to \infty$.

In Sect. V space-time information flow was probed with finite perturbations and measured with space-time averages $\langle X_{n\tau} \rangle$ [Eq. (18)]. This concept is somewhat opposite to the paradigm of Lyapunov exponents. For STC an infinitesimal perturbation will on average grow exponentially over time whereas finite perturbations measured through $\langle X_{n\tau} \rangle - \bar{X}_0$ decrease (somewhat) exponentially over time. On the one hand chaotic systems are sensitive to small changes in initial conditions, on the other hand initial conditions become qualitatively irrelevant over time as the finite differences eventually get lost in the dynamics of the system. The timescale associated with the decay of finite perturbations tells how quickly a system recovers from a large perturbation rather than how quickly a system diverges due to a small perturbation. Another important difference between finite and infinitesimal perturbations is that finite perturbations are fully expected to behave nonlinearly; i.e. the profile $\langle X_{n\tau} \rangle - \bar{X}_0$ should be nonlinear with regards to the perturbation $p(t)\mathbf{q}(n)$. For example, interference in the space-time information flow arises from a perturbation $\mathbf{q}(n)$ that describes two bump functions separated by a small spatial distance.

The techniques presented in this paper have been explored for reaction-diffusion networks and coupled map lattices, but they are applicable to a wide variety of systems such as extended systems without Laplacian diffusion (e.g. Lorenz-96 model) or fluids. For example, the information flow from the local scale to the mean field scale could be measured with finite perturbations (Sect. V), complementary to the reverse information flow studied in a globally coupled network [46]. With some modifications our techniques would also be applicable to delay differential equations. They could be extended to include higher order statistical moments besides the nodal average ($\langle X_n \rangle$). To some extent this was done in Figs. 2,3 and 4 for the variable a in the cGL network, since $\langle a_n \rangle = 0$ due to the $U(1)$ symmetry of the dynamical equation but $\left\langle a_n^2 \right\rangle \neq 0$. Even better would be the use of histograms to compute the probability distribution of a variable X at each node. The absolute difference (e.g. $|\langle X_n \rangle - \bar{X}_0|$) could then be replaced by a statistical distance between probability distributions. There is at least one advantage to this approach. Averages $\langle X_n \rangle$ are one-dimensional scalar quantities, and when compared against another scalar the error (e.g. $|\langle X_n \rangle - \bar{X}_0|$) can cross zero, which yields large dips in Fig. 3. Probability distributions should not have this problem since they are not scalar quantities; in addition they should be sensitive to a wider variety of changes in system behavior than simple averages.

ACKNOWLEDGMENTS

This research is based upon work supported by the National Science Foundation under grant number PHY-0653086, and by the Arctic Region Supercomputing Center at the University of Alaska Fairbanks as part of the Department of Defense High Performance Computing Modernization Program. R.W. thanks the Max-Planck Institute for Physics of Complex Systems for its hospitality.

[1] M.C. Cross and P.C Hohenberg, Rev. Mod. Phys. **65**, 851 (1993).

[2] W. Decker, W. Pesch, and A. Weber, Phys. Rev. Lett. **73**, 648 (1994); B. Echebarria and H. Riecke, Phys. Rev. Lett. **84**, 4838 (2000); K.E. Daniels and E. Bodenschatz, Phys. Rev. Lett. **88**, 034501(2002).

[3] Q. Ouyang and J.M. Flesselles, Nature **379**, 143 (1996).

[4] Z. Qu, J.N. Weiss, and A. Garfinkel, Phys. Rev. Lett. **78**, 1387 (1997).

[5] T. Tél and Y.C. Lai, Physics Reports **460**, 245 (2008).

[6] B. Hof, J. Westerweel, T.M. Schneider, and B. Eckhardt, Nature **443**, 59 (2006).

[7] A. Wacker, S. Bose, E. Schöll, Europhys. Lett. **31**, 257 (1995).

[8] M.C. Strain and H.S. Greenside, Phys. Rev. Lett. **80**, 2306 (1998).

[9] R. Wackerbauer, K. Showalter, Phys. Rev. Lett. **91**, 174103 (2003).

[10] E.N. Lorenz, *The Essence of Chaos*, (University of Washington Press, Seattle,1996).

[11] D.A. Egolf and H.S. Greenside, Nature **369**, 129 (1994).

[12] J.A. Vastano and H.L. Swinney, Phys. Rev. Lett. **60**, 1773 (1988).

[13] J.M. Nichols, Proc. R. Soc. B **272**, 871 (2005).

[14] T. Schreiber, Phys. Rev. Lett. **85**, 461 (2000).

[15] D. Ruelle, Commun. Math. Phys. **87**, 287 (1982).

[16] D. Ruelle, *Chaotic Evolution and Strange Attractors*, (Cambridge University Press, New York, 1989).

[17] S. Tajima and H. Greenside, Phys. Rev. E **66**, 017205 (2002).

[18] S.M. Houghton, E. Knobloch, S.M. Tobias, and M.R.E. Proctor, Phys. Lett. A **374**, 2030 (2010).

[19] H. Greenside, *Spatiotemporal Chaos in Large Systems: The Scaling of Complexity With Size*, CRM Proc. Lecture Notes **20**, 9 (1999).

[20] D. Stahlke and R. Wackerbauer, Phys. Rev. E **80**, 056211 (2009).

[21] S. Yonker S and R. Wackerbauer, Phys. Rev. E **73**, 026218 (2006)

[22] R. Wackerbauer, Phys. Rev. E **76**, 056207 (2007).

[23] R. Wackerbauer and S. Kobayashi, Phys. Rev. E **75**, 066209 (2007).

[24] J.P. Crutchfield and K. Kaneko, Phys. Rev. Lett. **60**, 2715 (1988).

[25] M. Fishman, D. Egolf, Phys. Rev. Lett. **96**, 054103 (2006).

[26] I.S. Aranson and L. Kramer, Rev. Mod. Phys. **74**, 99 (2002).

[27] P. Gray and S. K. Scott, Chem. Engin. Sci. 39, 1087 (1984).

[28] J.H. Merkin, V. Petrov, S.K. Scott and K. Showalter, Phys. Rev. Lett. **76**, 546 (1996).

[29] While N is used for network size in this paper, Fishman and Egolf use $L = N/\sqrt{D} = N/2$ [25].

[30] V.M. Eguiluz, P. Alstrom, E. Hernandez-Garcia, and O. Piro, Phys. Rev. E **59**, 2822 (1999).

[31] It is expected that $\langle X_n \rangle$ converges with an error proportional to $1/\sqrt{T}$, since the measured values X_n are rather uncorrelated in time due to the fast decay of temporal correlations in spatiotemporal chaos. Convergence is greatly improved by discarding the initial transient period during which the trajectory has not yet approached the chaotic attractor (cGL system) or the chaotic saddle (GS system), and by discarding the interval immediately preceding the collapse of spatiotemporal chaos.

[32] Non-chaotic exceptions in ring networks include stationary (or oscillatory) non-homogeneous spatial asymptotic states; for spatiotemporal chaos in ring networks we expect that $\langle X_n \rangle = \bar{X}$ for typical n [33], but we don't have a proof.

[33] R. Wackerbauer, H. Sun, and K. Showalter, Phys. Rev. Lett. **84**, 5018 (2000).

[34] Among the variables computed, the ones showing the greatest diversity of fluctuations were chosen for the plot. If the variable X is an odd power of $\langle da/dn \rangle$, the deviations are zero due to parity symmetry. In some cases of X a linear trend is easily seen and in others the limited range of N for which data is usable combined with the obfuscating fluctuations makes it difficult to measure a slope.

[35] Combining different variables improves the envelope. For example, consider the combination $\ln\left[\max_{X\in\{X^{(1)},X^{(2)},X^{(3)}\}}\left(s_X|\langle X_n\rangle - \bar{X}_0|\right)\right]$ where $X^{(1)}$, $X^{(2)}$, and $X^{(3)}$ are different variables, and s_X are subjectively chosen scale factors meant to compensate for the different characteristic magnitudes of the variables. This technique was used to generate the linear fit for the GS system depicted in Fig. 3c, using $X^{(1)} = a^2$, $X^{(2)} = da/dn$, and $X^{(3)} = r$. Among the variables computed, those showing the greatest variety in location of zero-crossing were chosen.

[36] For no-flux boundary conditions the local extinctions occasionally extend to the boundary node. In this case the excitation wave can only travel in from the side opposite to the boundary. The relative probability of excitation waves traveling in one direction vs. the other direction therefore also carries information about the proximity of a no-flux boundary.

[37] The Lyapunov spectrum was computed by integrating the linearized equations of motion and periodically orthonormalizing a set of perturbation vectors using the Gram-Schmidt method [38]. The Lyapunov dimension was computed from the Kaplan-Yorke formula [39], modified to use the integration of a spline fitted to the Lyapunov spectrum rather than a discrete sum. The graph of Lyapunov dimension $D_{\mathcal{L}}$ vs. number of nodes N was fitted to the equation $p_1 N + p_2 - p_3 \cos(2\pi N/p_4 + p_5)\exp(-N/p_6)$ with simulated annealing. A range of N spanning three oscillation wavelengths was used. The parameter p_6 corresponds to the decay length scale that is shown in Table I, and the parameter p_1 determines the chaotic length scale $1/p_1 = \xi_\delta$. The error function for the fitting used the sum of squares, with the errors weighted by $\exp(N/p_6')$ for a value of p_6' that was chosen to be close to the resultant p_6 value. In the case of $c_3 = 0.85$, sinusoidal fluctuations where not apparent and an ordinary linear fit was used to determine p_1 and p_2.

[38] T.S. Parker, L.O. Chua, *Practical Numerical Algorithms for Chaotic Systems*, Springer-Verlag, 1989.

[39] E. Ott, *Chaos in Dynamical Systems*, Cambridge University

Press, 2002.
[40] R. Shaw, Z. Naturforsch. **46a**, 80 (1981).
[41] A. Politi, R. Livi, G.-L. Oppo, R. Kapral, Europhys. Lett. **22**, 571 (1993).
[42] A. Politi and A. Torcini, ArXiv e-prints 0902.2545 (2009).
[43] Due to the discrete nature of time in this system, $w_t = 2$ corresponds to a perturbation that lasts for a single iteration, as can be seen by careful inspection of Eq. (15).
[44] A. Karimi and M.R. Paul, ArXiv e-prints 0906.3496 (2009).
[45] V.M. Eguiluz, E. Hernandez-Garcia, and O. Piro, Phys. Rev. E **64**, 036205 (2001).
[46] M. Escalona-Moran, G. Paredes, M.G. Cosenza, ArXiv e-prints 1010.4810 (2010)